ChemCatChem

ChemCatChem
Chemistry Europe
European Chemical Societies Publishing

RESEARCH ARTICLE OPEN ACCESS

Unexpected Oxidation of Co Nanoparticles Under H_2: X-Ray-Induced Water Radiolysis in NAP-XPS Studies

Sagar Sharma[1] | Michele De Rocco[1] | Martine Trentesaux[1] | Jean-Jacques Gallet[2,3] | Fabrice Bournel[2,3] | Ahmed Naitabdi[2] | Anne-Sophie Mamede[1] | Jean-François Paul[1] | Héloise Tissot[1]

[1]Univ. Lille, CNRS, Centrale Lille, Univ. Artois, UMR 8181–UCCS–Unité de Catalyse et Chimie du Solide, Lille, France | [2]Laboratoire de Chimie Physique-Matière Et Rayonnement, Sorbonne Université, Campus Curie, CNRS UMR, Paris, France | [3]Synchrotron SOLEIL, St. Aubin, France

Correspondence: Héloise Tissot (heloise.tissot@univ-lille.fr)

Received: 5 January 2026 | **Revised:** 5 May 2026 | **Accepted:** 20 May 2026

Keywords: beam damage | catalysis | near ambient pressure XPS | radiolysis

ABSTRACT

Cobalt nanoparticles exposed to 1 mbar H_2 during near-ambient-pressure x-ray photoelectron spectroscopy oxidize instead of reducing, a result that contradicts thermodynamic expectations. Using beam-free references, flux-dependent operando measurements, depth-resolved spectra, and thermal cycling, we show that x-ray radiolysis of trace water ($\sim 10^{-7}$ mbar) generates oxidizing species that dominate the surface chemistry of Co/SiO_2. This radiolytic pathway produces a reproducible kinetic steady state in which ~37% Co(II) persists even at 775 K under H_2, and it drives complete oxidation under CO due to the absence of a hydrogen-based reduction channel. Depth-dependent data confirm that this oxidation is surface-localized and directly controlled by photon flux, meaning the beam selectively modifies the layer that NAP-XPS is intended to probe. These results establish photon flux, background water, and thermal history as active reaction parameters and define general constraints for operando NAP-XPS on reducible, water-reactive metals.

1 | Introduction

Near-ambient-pressure x-ray photoelectron spectroscopy (NAP-XPS) is a key operando technique for probing catalytic surfaces under mbar-range gas environments. It provides direct information on oxidation states, adsorbates, and dynamic redox processes while maintaining surface sensitivity and chemical specificity. The method is widely applied to hydrogenation, CO conversion, Fischer–Tropsch synthesis, and reactions involving water [1, 2]. Synchrotron-based instruments further improve these capabilities by offering high signal-to-noise ratios, tunable photon energy, and the temporal resolution needed to track rapid changes in surface chemistry.

However, NAP-XPS measurements can be altered by x-ray-driven radiolysis of adsorbed or gas-phase species. In oxidizing or water-rich atmospheres, radiolysis produces highly reactive OH·, O·, and HO_2· radicals that can restructure metal and oxide surfaces at rates much faster than thermal processes. Beam-driven reactions of this type are also well documented in liquid and solid–liquid cells [2–6]. Even under nominally dry conditions, trace water at $\sim 10^{-7}$–10^{-5} mbar can initiate hydroxylation and oxidation cycles that obscure the intrinsic thermochemistry. Despite increasing recognition of these effects, most mechanistic studies have focused on oxidizing environments. Whether radiolysis also perturbs surface chemistry in strongly reducing gases such as H_2 or CO remains largely unresolved.

This question is particularly relevant for cobalt catalysts. In Fischer–Tropsch synthesis, metallic Co is the active phase, while water, an unavoidable product, has a debated role in oxidation, restructuring, and deactivation [7]. Co surfaces are highly sensi-

tive to water even at very low pressures, making them a suitable diagnostic system for separating the effects of intrinsic reduction, background water, and beam-generated oxidants. Resolving these contributions requires an operando technique with controlled photon flux, high spectral resolution, and surface-sensitive depth profiling, which synchrotron-based NAP-XPS can provide.

In this work, we use time-resolved NAP-XPS, tunable photon-flux control, and thermal cycling to isolate the competing pathways that determine the oxidation state of Co/SiO_2 nanoparticles under 1 mbar H_2 and CO. We show that trace water ($\sim 10^{-7}$ mbar) can generate beam-induced oxidizing species that dominate the observed surface chemistry, driving cobalt toward Co(II). By separating these beam-induced processes from genuine catalytic redox behavior, we develop a mechanistic framework for interpreting NAP-XPS data on water-reactive metals and provide practical guidelines and diagnostic criteria for minimizing artefacts in operando measurements.

2 | Materials and Experimental Methods

2.1 | Sample Preparation

Cobalt nanoparticles were deposited by electron-beam evaporation onto thermally oxidized Si(111) substrates. Sample preparation was performed in a UHV chamber (base pressure 10^{-10} mbar) connected to the catalysis chamber.

Substrate preparation: Si wafers were first degassed by stepwise heating to 800 K under $<1 \times 10^{-7}$ mbar, followed by a brief flash to 1000 K to remove residual contaminants. Thermal oxidation was then performed by exposing the substrate to 100 mbar O_2 at 960 K for 30 min. Formation of the SiO_2 layer was confirmed by Si 2p and O 1s photopeaks, and the oxide thickness was evaluated at ~6 nm from the intensity ratio between bulk Si and SiO_2 signals in the Si 2p spectrum.

Cobalt deposition: Metallic Co was deposited at room temperature in UHV using an electron-beam evaporator (emission 22 mA, flux 30 nA, 45 min). The deposition was monitored by XPS to control coverage and verify the metallic oxidation state. The Co film thickness was estimated at ~1 nm from the attenuation of the Si 2s signal before and after evaporation. However, this value represents an average equivalent thickness assuming a continuous film, whereas the actual Co deposit likely forms a discontinuous or island-type structure.

2.2 | NAP-XPS Measurements

NAP-XPS measurements were performed at the TEMPO beamline (SOLEIL Synchrotron) using a PHOIBOS 150-NAP analyzer (SPECS). Experiments were conducted under 1 mbar of H_2O, H_2, or CO. The sample was heated to 475 K in H_2O and to 775 K in H_2 or CO. Co 2p, O 1s, Si 2p, and Si 2s spectra were acquired primarily at $h\nu = 1050$ eV. Binding energies were referenced to metallic Co $2p_3/_2$ at 778.1 eV when metallic cobalt was present [8]. Typical acquisition times were ~100 s per spectrum.

The photon flux at the TEMPO beamline was monitored using a stainless-steel wire installed in the differentially pumped beam entrance, from which a drain current $I_0(h\nu)$ was measured. With an x-ray spot area of 8×10^{-3} mm^2, the maximum photon flux P_max reaches 1.3×10^{17} photons cm^{-2} s^{-1} at 200 eV. At $h\nu = 1050$ eV, a normalized flux of P/P_max = 3.7×10^{-3} was recorded, corresponding to an absolute photon flux of approximately 4.8×10^{14} photons cm^{-2} s^{-1}. Photon flux losses due to gas phase absorption along the ~5 cm beam path were negligible under the present pressure conditions (<10 mbar) [9]. Trace water was always present during operando measurements, with an estimated background pressure of 1–5×10^{-7} mbar based on base pressures obtained in previous experiments at this beamline. Fitting parameters are provided in the Supporting Information.

2.3 | Measurement Protocols

Three complementary protocols were used to separate thermal and beam-induced contributions:

(i) Ex situ reference measurements. Gas exposures (1 mbar H_2O at 475 K for 30 min and 1 mbar H_2 at 775 K for 1 h) were carried out without x-ray irradiation in the catalysis chamber. After cooling, samples were transferred under UHV to the analysis chamber. These spectra provide baseline thermochemical references.

(ii) Operando time-resolved measurements. Under continuous x-ray exposure, sequential Co 2p spectra were collected at fixed temperature and pressure to monitor time-dependent oxidation or reduction. Cooling from 775 K to 300–340 K was achieved by switching off the heater while maintaining gas flow and beam irradiation.

(iii) Flux-dependent measurements. The same thermal and gas-exposure sequences were repeated at two photon-flux levels that differed by a factor of 15 to evaluate how oxidation kinetics depend on beam intensity.

3 | Results

3.1 | Water-Induced Oxidation and Reference Spectra

Exposure of metallic Co to water and hydrogen in the absence of x-ray irradiation (experiment follows protocol (i), Figure 1) shows how the material responds under beam-free conditions. The as-deposited film exhibits a clean metallic Co $2p_{3/2}$ peak at 778.1 eV, confirming formation of a fully metallic state by electron-beam evaporation. Subsequent exposure to 1 mbar H_2O at 475 K for 30 min converts this spectrum into the characteristic $CoO/Co(OH)_2$ fingerprint with components at 780.0, 781.1, and 785.1 eV (Fitted spectra and Fitting details are presented in Figure S1 using Biesenger et al. results from ref [8]). No Co_3O_4 features appear, indicating that water alone drives direct hydroxylation rather than oxide formation. This establishes the high reactivity of Co toward water and defines the oxidized $CoO/Co(OH)_2$ reference spectrum used in later assignments.

The ability of H_2 at high temperature to restore a metallic surface under beam-free conditions was then evaluated. After treatment in 1 mbar H_2 at 775 K for 1 h, the spectrum contains both the

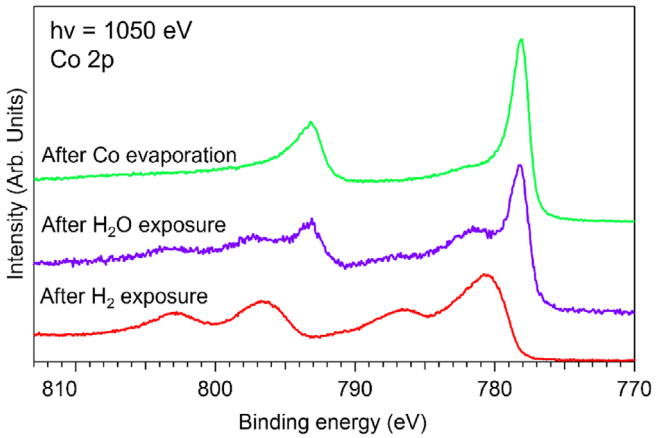

FIGURE 1 | Co 2p spectra as prepared just after Co evaporation (green), after exposure to 1 mbar water during 30 min at 475 K (violet), after exposure to 1 mbar H_2 during 60 min at 775 K (red), spectra are collected in UHV at RT. Experiment follows protocol (i).

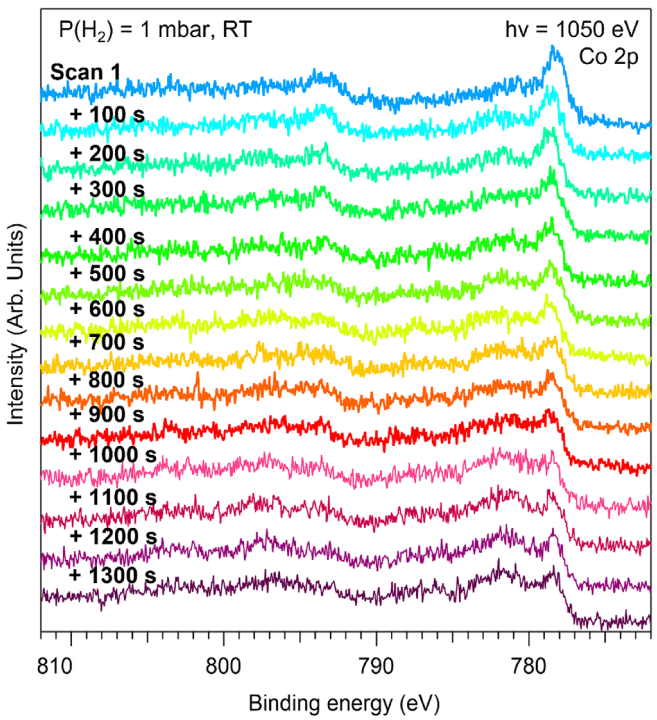

FIGURE 2 | Time dependance Co 2p spectra evolution under 1 mbar H_2 at 300 K. The sample was pretreated by heating to 775 K in 1 mbar H_2 for 60 min, then cooled to ~300 K (30 min waiting period) before acquiring scan 1. Experiment follows protocol (ii).

778.1 eV metallic peak and residual $CoO/Co(OH)_2$ accounting for ~37% of the total Co signal. Even at high temperature, the hydroxylated fraction persists, indicating that trace water at $\sim 10^{-7}$ mbar remaining from the prior H_2O exposure or desorbing from chamber walls during heating imposes a lower bound on the metallic fraction. Consequently, the "metallic" reference state accessible in NAP-XPS is inherently and reproducibly partially hydroxylated before any beam exposure.

These observations set the baseline for interpreting operando spectra. If water alone fixes ~37% Co(II) under H_2 reduction,

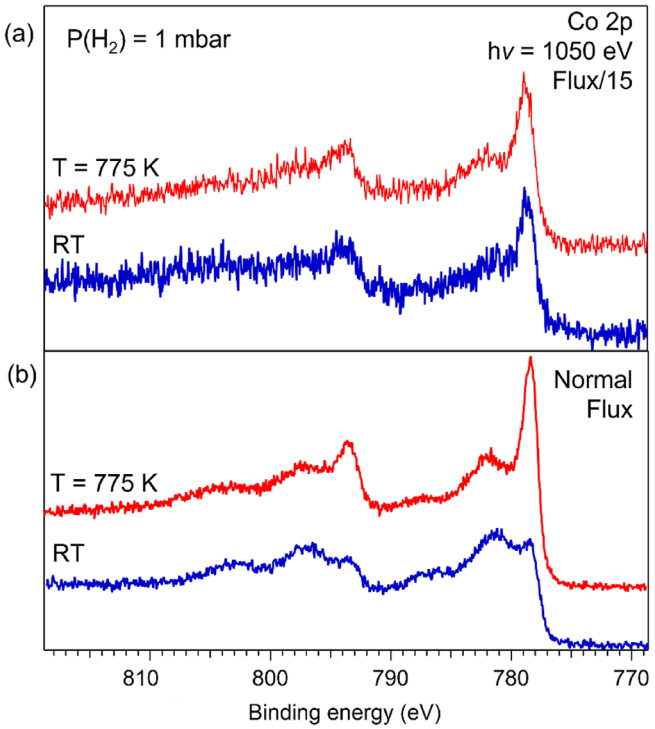

FIGURE 3 | Flux dependence of Co 2p spectra. The same procedure as in Figure 1 was performed at two different x-ray beam fluxes. For (a), the flux was divided by 15 compared to (b). Red spectra were acquired in 1 mbar H_2 at 775 K. Blue spectra were acquired after a time delay of 25 min for (a) and 30 min for (b) under x-ray irradiation following cessation of heating (cooling down to 300 K). The total photon dose received during the waiting period differs by a factor of approximately 18 between the two experiments. Experiment follows protocol (iii).

additional oxidizing flux generated by x-ray irradiation has the potential to shift the Co(0)/Co(II) balance far beyond this thermochemical limit. The onset and magnitude of this beam-driven oxidation are addressed in Figure 2.

3.2 | Beam-Induced Oxidation Under H_2: Time and Flux Dependence

Figure 2 shows how the Co surface evolves under 1 mbar H_2 at ~300 K when the x-ray beam is on. The first spectrum, collected after reduction at 775 K and cooling for 30 min, contains the expected metallic peak with ~37% $CoO/Co(OH)_2$. Successive scans reveal a gradual increase in the high-binding-energy feature at ~782 eV, indicating progressive oxidation despite the reducing atmosphere at room temperature. This behavior demonstrates that oxidation of surface Co into $CoO/Co(OH)_2$ by residual water proceeds faster than H_2 can reduce it, shifting the surface equilibrium toward $CoO/Co(OH)_2$ even at room temperature.

To determine the origin of this oxidation, whether driven solely by residual water or enhanced by x-ray-induced processes, we tested the role of photon flux by repeating the experiment for two beam intensities (Figure 3). At 775 K, both conditions produce the same mixed Co(0)/Co(II) state, confirming identical starting points. After cooling, the spectra diverge. Under low flux (Flux/15, see Figure 3a), the $CoO/Co(OH)_2$ fraction remains

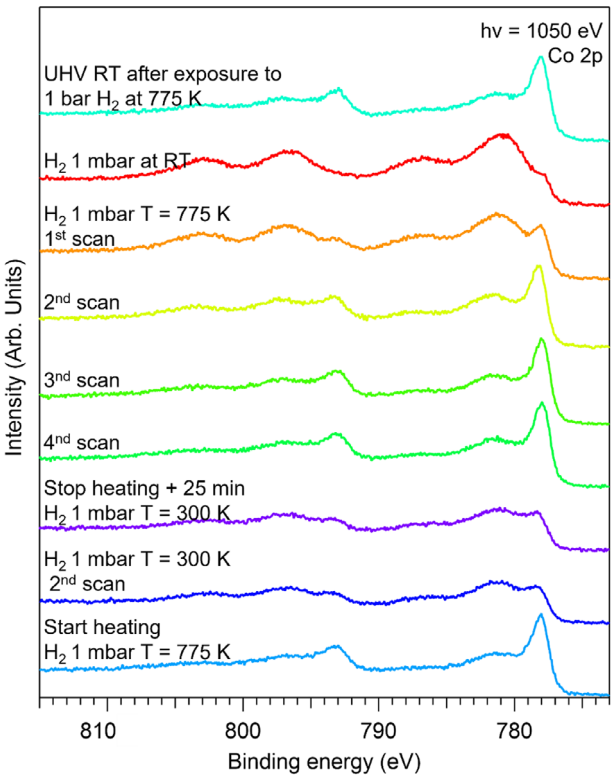

FIGURE 4 | Temperature dependence of Co 2p spectra evolution during thermal cycling in 1 mbar H_2. The red spectrum serves as the starting point, acquired at room temperature upon initial H_2 exposure, and shows a partially oxidized Co surface. Sequential spectra acquired during heating to 775 K (orange, yellow, light green, and green) reveal a progressive increase in the metallic Co(0) fraction as temperature rises, reflecting H_2-driven reduction. However, even at 775 K, the system converges to a stable mixed Co(0)/Co(II) state (~63/37 ratio) rather than achieving complete reduction. Upon cooling back to 300 K (purple and dark blue), the Co(II) fraction increases again, demonstrating that the reduction is not irreversible and that reoxidation occurs during cooling. Reheating (light blue) partially restores the metallic fraction, confirming the reversible nature of this temperature-dependent redox cycling. The cyan spectrum, acquired in UHV at room temperature after H_2 exposure, is shown as a reference. All spectra illustrate the competition between H_2-driven reduction and continuous re-oxidation by trace water and radiolysis products. (1 scan = 100 s). Experiment follows protocol (i).

near the ~37% baseline. Under normal flux (see Figure 3b), the oxidized component grows to ~_80% of the total Co signal. This flux dependence demonstrates that the oxidation kinetics are beam-controlled: increased photon flux generates more radiolysis events per unit time, accelerating hydroxylation far beyond the limit imposed by background water. These results establish a causal link between beam intensity and oxidation rate, motivating the temperature-dependent analysis presented in Figure 4.

3.3 | Temperature-Dependent Competition and Steady State Under H_2

Figure 4 shows the evolution of the Co 2p spectrum during thermal cycling in 1 mbar H_2. After reduction at 775 K, exposure to H_2 at room temperature yields a strongly oxidized spectrum

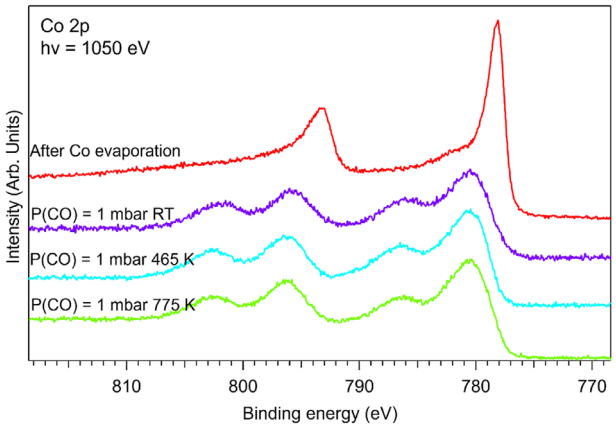

FIGURE 5 | Co 2p spectra evolution under 1 mbar CO at different temperatures. Spectra acquired after Co evaporation (red), under 1 mbar CO at room temperature (violet), at 465 K (cyan), and at 775 K (green).

with ~85% Co(II) (see Figure S3). Heating this state back to 775 K progressively decreases the $CoO/Co(OH)_2$ contribution, and after several scans the spectrum stabilizes at a mixed state resembling the reduced reference. Cooling to ~300 K restores a larger hydroxide fraction, and reheating again returns the system to the same mixed state. These cycles indicate a reproducible balance between H_2-driven reduction at elevated temperature and continuous re-oxidation by residual water and beam-generated oxidants.

Depth-dependent measurements (Figure S2) show that this oxidation is confined to a near-surface region. Surface-sensitive spectra (lower kinetic energy) contain a larger $CoO/Co(OH)_2$ contribution than bulk-sensitive spectra, while the metallic component is more pronounced at higher kinetic energy. The oxidation observed under H_2 therefore corresponds to a thin hydroxylated surface rather than a bulk transformation, meaning the beam-water artefact selectively modifies the surface layer that NAP-XPS probes.

Quantitative analysis of the thermal-cycling spectra (Figure S3) shows that the Co(0) fraction increases with temperature and converges toward a plateau of ~63% Co(0) and 37% Co(II) at 775 K. The system does not approach a fully metallic state; instead, it consistently returns to this 63/37 ratio under fixed H_2 flow and beam conditions. This behavior represents a kinetic steady state produced by the competition between temperature-enhanced H_2 reduction and persistent re-oxidation by water and radiolysis products. The resulting Co(0)/Co(II) ratio therefore reflects measurement-condition dependent kinetics rather than the intrinsic catalytic equilibrium dictated solely by the gas phase. The robustness of this plateau motivates the comparison with CO in Figure 5.

3.4 | CO Versus H_2: When Oxidation Completely Dominates

Figure 5 shows the evolution of the Co 2p spectrum under 1 mbar CO from room temperature to 775 K. After establishing the metallic reference, exposure to CO at any temperature

results in the same hydroxylated profile observed after direct water exposure, with the $CoO/Co(OH)_2$ component dominating the spectrum. Neither higher temperature nor longer exposure recovers any detectable metallic Co. CO therefore provides no effective reduction pathway capable of counteracting oxidation by residual water and beam-generated species.

This behavior represents the extreme limit of the beam–water artefact. Under H_2, a kinetic balance forms in which ~37% Co(II) persists even at high temperature because H_2-driven reduction and radiolysis-driven re-oxidation compete: H_2 supplies atomic hydrogen capable of scavenging surface OH species generated by water radiolysis. Under CO, no such balance exists. Although CO is known to reduce metal oxides under dry conditions, it cannot provide atomic hydrogen to remove surface OH species, and therefore offers no effective competition against the continuous oxidizing environment created by water radiolysis. As a result, the surface is driven entirely to Co(II) across the full temperature range. The position of the Co(0)/Co(II) steady state therefore does not reflect a weaker reducing power of CO in general, but rather its inability to counteract radiolysis-derived hydroxyl species specifically in water-prone environments. These results show that operando NAP-XPS can yield fully misleading oxidation states for metals that lack a hydrogen-based reduction channel under such conditions.

This behavior represents the extreme limit of the beam–water artefact. Under H_2, a kinetic balance forms in which ~37% Co(II) persists even at high temperature because H_2-driven reduction and radiolysis-driven re-oxidation compete: H_2 supplies atomic hydrogen capable of scavenging surface OH species generated by water radiolysis. Molecular hydrogen dissociates on metallic Co(0) sites to yield surface-bound atomic hydrogen (H*) [16], which reacts with surface OH groups to regenerate water [15]. (X-ray irradiation could in principle also generate H• radicals by radiolysis of H_2, this contribution is expected to be negligible given the much lower photoionization cross-section of H_2 compared to H_2O at 1050 eV.) Under CO, no such balance exists. Although CO is known to reduce metal oxides under dry conditions, it cannot provide atomic hydrogen to remove surface OH species, and therefore offers no effective competition against the continuous oxidizing environment created by water radiolysis. As a result, the surface is driven entirely to Co(II) across the full temperature range. The position of the Co(0)/Co(II) steady state therefore does not reflect a weaker reducing power of CO in general, but rather its inability to counteract radiolysis-derived hydroxyl species specifically in water-prone environments. These results show that operando NAP-XPS can yield fully misleading oxidation states for metals that lack a hydrogen-based reduction channel under such conditions.

4 | Discussion

4.1 | Mechanistic Picture of Beam-Induced Co Oxidation Under NAP-XPS

Beam-induced oxidation of Co under NAP-XPS results from the combined influence of baseline oxidation by trace water and an additional oxidizing environment created by x-ray radiolysis. Even without irradiation, water is an efficient oxidant for cobalt. Exposure to 1 mbar H_2O at 475 K produces a fully oxydized $CoO/Co(OH)_2$ spectrum, consistent with reports that water dissociates readily on Co(0001) and oxidizes Co surfaces at pressures as low as 10^{-7}–10^{-5} mbar [10]. The persistence of ~37% Co(II) after reduction in 1 mbar H_2 at 775 K reflects the same limitation: cobalt oxides are difficult to fully reduce when water is present [10]. Prior studies by Kizilkaya, Ernst, Morales, and Wu attribute incomplete reduction to re-oxidation by water formed or released during heating and cooling [10–13]. Thus, even before the beam is applied, trace water establishes a structural baseline in which the "metallic" Co state accessible in NAP-XPS is intrinsically and reproducibly partially hydroxylated. Furthermore, the hydroxyl film appears to reach a reproducible coverage, suggesting it forms a passivation layer under these conditions.

When the x-ray beam is introduced, this baseline oxidation is amplified through radiolysis of residual water. At room temperature in 1 mbar H_2, surfaces that initially contain ~37% Co(II) become progressively more oxidized with each scan, and the extent of oxidation scales with photon flux. Such behavior cannot be accounted for by H_2/H_2O thermodynamics and is consistent with the formation of reactive oxidizing species such as OH· and H_2O_2 under irradiation. Temperature cycling in H_2 further illustrates the competition between these processes. Heating increases the metallic fraction as H_2 reduces oxygen-containing species and helps remove water, but even at 775 K the system converges to a stable ~63/37 Co(0)/Co(II) ratio. Cooling re-establishes a higher hydroxide fraction. This plateau represents a kinetic steady state governed by opposing fluxes, H_2-driven reduction versus continuous re-oxidation by water and radiolysis products, rather than an intrinsic equilibrium.

Other beam-induced effects, such as local heating and secondary-electron-driven chemistry, were also considered. Although SiO_2 has a lower thermal conductivity than metallic substrates, significant local temperature rises are unlikely at the photon flux used in the present experiments. Furthermore, beam-induced heating would be expected to promote the thermally driven reduction of CoO under H_2 atmosphere, which is contrary to the oxidation behavior we observe, allowing us to rule out heating as a contributing mechanism. Regarding secondary-electron-driven chemistry, secondary electrons generated by x-ray photoionization are well-known intermediates in the radiolysis of water molecules, producing reactive •OH radicals, and their contribution is therefore inherently included in the radiolysis mechanism discussed above. While we attempted to decouple the respective contributions of secondary electrons and direct photon-induced ionization, both phenomena are deeply intertwined and could not be separated experimentally.

The comparison with CO shows the extreme limit of this competition. Although CO can reduce cobalt oxides under dry conditions and has been reported to maintain metallic Co more effectively than H_2 in the absence of water, these advantages vanish when trace water is present. Prior studies demonstrate that even small amounts of water oxidize metallic Co at room temperature, particularly on stepped or nanoparticle surfaces [14–16]. In agreement with this behavior, NAP-XPS measurements in 1 mbar CO yield a fully hydroxylated spectrum from room temperature to 775 K, with no detectable metallic Co [10]. The mechanistic origin is

straightforward: CO does not provide hydrogen to remove surface OH species, so once radiolysis supplies additional oxidizing environment, CO offers no competing reduction pathway. The surface therefore collapses entirely to Co(II).

Taken together, these observations define a consistent mechanistic picture. Residual water imposes a minimum oxidation level; the x-ray beam amplifies this oxidation through radiolysis; H_2 can partially counteract the resulting oxidative environment by supplying atomic hydrogen, whereas CO cannot [6]. Under H_2, the system therefore adopts a flux- and temperature-dependent mixed Co(0)/Co(II) steady state, while under CO it is driven to complete oxidation across the accessible temperature range.

4.2 | Generalization and Limitations

The scope of the present study is intentionally limited, and the conclusions should be interpreted within this context. In particular, the reproducible Co(0)/Co(II) ratio of ~63/37 observed at 775 K under 1 mbar H_2 should not be considered a universal value but rather a system-specific steady state. Cobalt reducibility is known to depend strongly on particle size, morphology, and metal-support interactions: Castner et al. demonstrated that the reduction of Co^{2+} to Co^0 on silica-supported catalysts is highly sensitive to these parameters [17], with reduction temperatures differing by up to 150 K across three different silica supports. Kiennemann et al. similarly reported that for a 25 wt% Co/SiO_2 catalyst reduced at 773 K, the Co 2p spectrum could only be decomposed into metallic cobalt (82%) and CoO (18%), confirming that complete reduction of silica-supported Co is rarely achieved even at elevated temperatures [11]. Furthermore, Wu et al. showed on cobalt foil that H_2 is a significantly less efficient reductant than CO, requiring temperatures approximately 100°C higher to achieve full reduction [10].

Beyond the specifics of the Co/SiO_2 system, the mechanistic features identified for Co baseline oxidation by trace water and beam-amplified re-oxidation via radiolysis are consistent with a broad range of observations across metal-gas and metal-water interfaces. Beam-accelerated oxidation has been reported for Au exposed to O_2, where surfaces remain stable for hours without irradiation but oxidize rapidly once the x-ray beam is applied [18, 19]. Similar behavior at much lower photon fluxes has been documented on Au and other metals using laboratory sources [20], demonstrating that the effect is not restricted to synchrotron intensities. Pt exhibits beam-driven oxide formation on Pt(110) [21], and Cu surfaces are particularly susceptible: Cu nanoparticles oxidize more strongly under continuous irradiation than during delayed measurements, showing that x-ray ionization of O_2 enhances the oxidizing environment [22]. In contrast, under UHV conditions, copper oxides are reduced by the beam, highlighting the critical role of gas-phase composition in determining beam-induced chemistry. Beam-induced molecular transformations also occur, such as carbonate formation during CO_2 activation on Cu [23]. Related effects appear even in nominally reducing environments, as seen for ceria under H_2 at high temperature, where both gas-phase chemistry and irradiation contributed to the observed state [24]. Together, these studies indicate that x-ray–driven chemical modification is widespread whenever reactive gases or water-derived species are present, placing the Co/H_2–H_2O system studied here within a larger class of water-susceptible materials.

Water radiolysis phenomena at solid–liquid interfaces reinforce this broader generality. Cu electrodes oxidize under x-ray exposure in air or alkaline solution due to rapid formation of radiolysis products [22], and Pt thin films show flux-dependent reduction of Pt^{4+}/Pt^{2+} species under a few millibar of water vapor [25]. Hydrated solids demonstrate even more pronounced effects: aqueous NaCl/NaBr/NaI droplets generate unexpected oxidized halogen species under irradiation [9]; chloride-containing LDHs form ClO^- and ultimately ClO_4^-; and hydrated smectite clays mineralize intercalated pyridine to N_2 [26, 27]. Ion migration has also been observed in hydrated phyllosilicates at relative humidities above ~50% [28, 29]. Across these systems, the underlying principle is the same: whenever water is present, adsorbed, confined, or in the gas phase, x-ray irradiation generates highly reactive species capable of significantly modifying surface chemistry. The behavior of Co/SiO_2 under NAP-XPS therefore fits directly into this radiolysis-driven framework.

The scope of the present study is intentionally limited, and the conclusions should be interpreted within this context. A single metal/support system (Co/SiO_2) was examined over a restricted pressure range (1 mbar H_2, H_2O, CO), without variation in particle size, support chemistry, photon energy, or humidity. Radiolysis products were not quantified, their kinetics were not measured directly, and no mechanistic or microkinetic model was constructed to describe the competing reduction and oxidation pathways. The identity and concentration of beam-generated species therefore remain inferred rather than experimentally resolved. Depth-dependent NAP-XPS indicates that oxidation is confined to a near-surface region, but this observation was not corroborated with independent structural probes. Finally, although parallels across Au, Pt, Cu, LDH, and aqueous systems strongly suggest that radiolysis-driven chemistry is general, the quantitative extent of beam influence is system-dependent. Extrapolation to other metals, supports, or pressure regimes should therefore be made cautiously, particularly where water binding energetics, gas composition, or radiolysis susceptibility differ from the Co/H_2-H_2O conditions studied here.

4.3 | Practical Implications for NAP-XPS on Reducible Metals

The results of this study demonstrate that NAP-XPS can significantly perturb the oxidation state of reducible metals when trace water is present, because x-ray irradiation introduces an additional, flux-dependent oxidizing pathway that directly competes with thermal reduction. For Co/SiO_2, this produces a surface-localized Co(II) fraction that cannot be removed by heating alone and can increase during data acquisition, potentially mimicking or obscuring genuine catalytic steady states. Because similar radiolysis-driven changes have been reported for Au, Pt, Cu, CeO_2, and hydrated solids, these effects should be considered a general concern for operando measurements in water-prone environments [18, 19, 21, 22, 24].

This mechanistic understanding places specific demands on experimental design in NAP-XPS studies of reducible metals.

Key parameters that influence the observed oxidation state include photon flux, residual water introduced through gas delivery or thermal treatments, the sequence and duration of heating and cooling steps, the choice of gas environment (e.g., CO versus H_2), and the number and depth-sensitivity of repeated scans. Each of these variables can shift the oxidation–reduction balance in predictable but system-dependent ways, meaning that correct operando interpretation requires explicit evaluation of how measurement conditions shape the recorded spectra.

To ensure reliable data interpretation, several practices should become standard: flux measurement to have an idea of the irradiation dose rate, mass spectrometer use to control the composition of the gas phase (water presence, unexpected produced species), systematic comparison of successive scans to identify spectral shifts and peak broadening, control experiments without x-ray exposure to distinguish beam-induced artifacts from genuine chemical transformations, and analysis of multiple sample spots to assess the spatial extent of beam damage. When needed, depending on the project goal, rigorous chamber cleanliness with extended baking procedures is essential to minimize background water contamination.

5 | Conclusion

This work shows that NAP-XPS measurements on reducible metals can be substantially altered by x-ray radiolysis of trace water, which introduces a competing oxidative pathway that obscures the intrinsic redox chemistry of the catalyst. For Co/SiO_2, representative of Fischer–Tropsch systems, we identify kinetic limits such as a persistent ~37% Co(II) fraction under H_2 and complete oxidation under CO. These states originate not from gas-phase thermodynamics but from a measurable balance between thermal reduction and radiolysis-driven re-oxidation and therefore reflect measurement conditions rather than true operando behavior.

Mechanistically, continuous generation of OH·, O·, and peroxide species under irradiation re-oxidizes metallic Co faster than H_2 or CO can remove oxygen. Similar radiolysis-driven effects reported for Au, Pt, Cu, CeO_2, and hydrated solids indicate that this behavior is general for water-susceptible materials studied under near-ambient pressures.

These findings underscore the need to treat photon flux, residual water, and thermal history as active reaction parameters in operando NAP-XPS. Flux-minimized, humidity-controlled, and beam-on/beam-off benchmarking protocols are essential to prevent beam artefacts from being misinterpreted as catalytic steady states.

Acknowledgments

The authors acknowledge Synchrotron SOLEIL for provision of beamtime on the TEMPO beamline (proposal BAG 20140465). The authors thank La Maison de la Chimie for financial support of the postdoctoral fellowship of Sagar Sharma. The authors acknowledge the ANR for funding of project BLAN08-1_315088 "Surfaces under Ambient Pressure with Electron Spectroscopies".

Open access publication funding provided by COUPERIN CY26.

Conflicts of Interest

The authors declare no conflicts of interest.

Data Availability Statement

The data that support the findings of this study are available from the corresponding author upon reasonable request.

References

1. L. Zhong, D. Chen, and S. Zafeiratos, "A Mini Review of In Situ Near-Ambient Pressure XPS Studies on Non-Noble, Late Transition Metal Catalysts," *Catalysis Science & Technology* 9 (2019): 3851–3867, https://doi.org/10.1039/C9CY00632J.

2. F. D. Ogletree, H. Bluhm, E. D. Hebenstreit, and M. Salmeron, "Photoelectron Spectroscopy Under Ambient Pressure and Temperature Conditions," *Nuclear Instruments and Methods in Physics Research Section A: Accelerators, Spectrometers, Detectors and Associated Equipment* 601 (2009): 151–160, https://doi.org/10.1016/j.nima.2008.12.155.

3. B. Rotonnelli, M.-S. D. Fernandes, F. Bournel, J.-J. Gallet, and B. Lassalle-Kaiser, "In Situ/Operando X-Ray Absorption and Photoelectron Spectroscopies Applied to Water-Splitting Electrocatalysis," *Current Opinion in Electrochemistry* 40 (2023): 101314.

4. R. Dupuy, C. Richter, B. Winter, G. Meijer, R. Schlögl, and H. Bluhm, "Core Level Photoelectron Spectroscopy of Heterogeneous Reactions at liquid–Vapor Interfaces: Current Status, Challenges, and Prospects," *Journal of Chemical Physics* 154 (2021): 060901, https://doi.org/10.1063/5.0036178.

5. S. Axnanda, E. J. Crumlin, B. Mao, et al., "Using "Tender" X-Ray Ambient Pressure X-Ray Photoelectron Spectroscopy as A Direct Probe of Solid-Liquid Interface," *Scientific Reports* 5 (2015): 9788, https://doi.org/10.1038/srep09788.

6. C. Arble, H. Guo, E. Strelcov, et al., "Radiation Damage of Liquid Electrolyte During Focused X-Ray Beam Photoelectron Spectroscopy," *Surface Science* 697 (2020): 121608, https://doi.org/10.1016/j.susc.2020.121608.

7. A. Y. Khodakov, "Fischer-Tropsch Synthesis: Relations Between Structure of Cobalt Catalysts and Their Catalytic Performance," *Catalysis Today* 144 (2009): 251–257, https://doi.org/10.1016/j.cattod.2008.10.036.

8. M. C. Biesinger, B. P. Payne, A. P. Grosvenor, L. W. M. Lau, A. R. Gerson, and R. S. C. Smart, "Resolving Surface Chemical States in XPS Analysis of First Row Transition Metals, Oxides and Hydroxides: Cr, Mn, Fe, Co and Ni," *Applied Surface Science* 257 (2011): 2717–2730, https://doi.org/10.1016/j.apsusc.2010.10.051.

9. L. Xu, Y. Ma, Y. Zhang, et al., "Water Adsorption on a Co(0001) Surface," *Journal of Physical Chemistry C* 114 (2010): 17023–17029, https://doi.org/10.1021/jp102788x.

10. C. H. Wu, B. Eren, H. Bluhm, and M. B. Salmeron, "Ambient-Pressure X-Ray Photoelectron Spectroscopy Study of Cobalt Foil Model Catalyst Under CO, H_2, and Their Mixtures," *ACS Catalysis* 7 (2017): 1150–1157, https://doi.org/10.1021/acscatal.6b02835.

11. A. Galtayries and J. Grimblot, "Formation and Electronic Properties of Oxide and Sulphide Films of Co, Ni and Mo Studied by XPS, Ni and Mo Studied by XPS," *Journal of Electron Spectroscopy and Related Phenomena* 98–99 (1999): 267–275, https://doi.org/10.1016/S0368-2048(98)00292-8.

12. B. Ernst, A. Bensaddik, L. Hilaire, P. Chaumette, and A. Kiennemann, "Study on a Cobalt Silica Catalyst During Reduction and Fischer-Tropsch Reaction: In Situ EXAFS Compared to XPS and XRD," *Catalysis Today* 39 (1998): 329–341.

13. F. Morales, F. M. F. De Groot, P. Glatzel, et al., "In Situ X-Ray Absorption of Co/Mn/TiO_2 Catalysts for Fischer-Tropsch Synthesis," *Journal of Physical Chemistry B* 108 (2004): 16201–16207.

14. A. C. Kizilkaya, J. W. Niemantsverdriet, and C. J. Weststrate, "Oxygen Adsorption and Water Formation on Co(0001)," *Journal of Physical Chemistry C* 120 (2016): 4833–4842, https://doi.org/10.1021/acs.jpcc.5b08959.

15. C. J. Weststrate, D. Sharma, M. A. Gleeson, and J. W. Niemantsverdriet, "Water and Hydroxyl Reactivity on Flat and Stepped Cobalt Surfaces," *Journal of Physical Chemistry C* 127 (2023): 2974–2980, https://doi.org/10.1021/acs.jpcc.2c08425.

16. C. J. Weststrate, D. Sharma, D. Rodriguez-Padron, M. A. Gleeson, H. O. A. Fredriksson, and J. W. Niemantsverdriet, "Spectroscopic Investigation of a Co(0001) Model Catalyst During Exposure to H_2 and CO at Near-Ambient Pressures," *Physical Chemistry Chemical Physics* 25 (2023): 23053–23061.

17. P. J. Van Berge, J. Van De Loosdrecht, S. Barradas, and A. M. Van Der Kraan, "Oxidation of Cobalt Based Fischer–Tropsch Catalysts as a Deactivation Mechanism," *Catalysis Today* 58 (2000): 321–334.

18. N. Jiang, "Electron Beam Damage in Oxides: A Review," *Reports on Progress in Physics* 79 (2016): 016501, https://doi.org/10.1088/0034-4885/79/1/016501.

19. P. Jiang, S. Porsgaard, F. Borondics, et al., "Room-Temperature Reaction of Oxygen With Gold: An in Situ Ambient-Pressure X-Ray Photoelectron Spectroscopy Investigation," *Journal of the American Chemical Society* 132 (2010): 2858–2859, https://doi.org/10.1021/ja909987j.

20. K. Dumbuya, G. Cabailh, R. Lazzari, et al., "Evidence for an Active Oxygen Species on Au/TiO2(110) Model Catalysts During Investigation with in Situ X-Ray Photoelectron Spectroscopy," *Catalysis Today* 181 (2012): 20–25.

21. D. R. Butcher, M. E. Grass, Z. Zeng, et al., "In Situ Oxidation Study of Pt(110) and Its Interaction With CO," *Journal of the American Chemical Society* 133 (2011): 20319–20325, https://doi.org/10.1021/ja207261s.

22. R. S. Weatherup, C. H. Wu, C. Escudero, V. Pérez-Dieste, and M. B. Salmeron, "Environment-Dependent Radiation Damage in Atmospheric Pressure X-Ray Spectroscopy," *Journal of Physical Chemistry B* 122 (2018): 737–744, https://doi.org/10.1021/acs.jpcb.7b06397.

23. X. Deng, A. Verdaguer, T. Herranz, C. Weis, H. Bluhm, and M. Salmeron, "Surface Chemistry of Cu in the Presence of CO_2 and H_2O," *Langmuir* 24 (2008): 9474–9478, https://doi.org/10.1021/la8011052.

24. W. T. Figueiredo, C. Escudero, V. Pérez-Dieste, C. A. Ospina, and F. Bernardi, "Determining the Surface Atomic Population of Cu_xNi_{1-x}/CeO_2 ($0 < x \leq 1$) Nanoparticles During Reverse Water-Gas Shift (RWGS) Reaction," *Journal of Catalysis* 365 (2018): 174–184.

25. J. Fraxedas, K. Zhang, B. Sepúlveda, et al., "Water-Mediated Photo-Induced Reduction of Platinum Films," *Journal of Synchrotron Radiation* 26 (2019): 1288–1293, https://doi.org/10.1107/S1600577519004685.

26. H. Tissot, R. Coustel, F. Rochet, et al., "Deciphering Radiolytic Oxidation in Halide Aqueous Solutions: A Pathway Toward Improved Synchrotron NAP-XPS Analysis," *Journal of Physical Chemistry C* 127 (2023): 15825–15838, https://doi.org/10.1021/acs.jpcc.3c03676.

27. R. Coustel, A. Boucly, E. André, et al., "NAP-XPS Probes the Electronic Structure of the Mg–Al–Cl Layered Double Hydroxide upon Controlled Hydration," *Journal of Physical Chemistry C* 127 (2023): 4144–4153, https://doi.org/10.1021/acs.jpcc.2c05362.

28. A. Boucly, F. Rochet, Q. Arnoux, et al., "Soft X-Ray Heterogeneous Radiolysis of Pyridine in the Presence of Hydrated Strontium-Hydroxyhectorite and Its Monitoring by Near-Ambient Pressure Photoelectron Spectroscopy," *Scientific Reports* 8 (2018): 6439.

29. A. Boucly, F. Rochet, H. Tissot, et al., "Electronic Structure Sensitivity to Hydration in Smectite Clays Unveiled by Near-Ambient Pressure X-Ray Photoelectron Spectroscopy," *Journal of Physical Chemistry C* 128 (2024): 17112–17123.

Supporting Information

Additional supporting information can be found online in the Supporting Information section.

Supporting File: cctc70826-sup-0001-SuppMat.docx.